Theoretical approaches in adsorption: alkali adatom investigations

2007 J. Phys.: Condens. Matter 19 305005

(http://iopscience.iop.org/0953-8984/19/30/305005)

IOP PUBLISHING JOURNAL OF PHYSICS: CONDENSED MATTER

J. Phys.: Condens. Matter **19** (2007) 305005 (17pp) doi:10.1088/0953-8984/19/30/305005

TOPICAL REVIEW

Theoretical approaches in adsorption: alkali adatom investigations

G P Brivio[1], G Butti[1], S Caravati[1], G Fratesi[1,2] and M I Trioni[3]

[1] CNISM and Dipartimento di Scienza dei Materiali, Università di Milano-Bicocca, Via Cozzi 53, 20125 Milano, Italy
[2] ETSF and Dipartimento di Fisica, Università di Milano, Via Celoria 16, 20133 Milano, Italy
[3] CNISM, UdR Milano-Bicocca, Via Cozzi 53, 20125 Milano, Italy

E-mail: gianpaolo.brivio@unimib.it

Received 5 February 2007, in final form 28 February 2007
Published 13 July 2007
Online at stacks.iop.org/JPhysCM/19/305005

Abstract

We discuss how different properties at surfaces could require for different theoretical treatments within the first-principles density functional theory. Energies and structures are accurately determined by adopting the supercell geometry. Surface states are more conveniently described by the Green function embedding approach, which is able to take into account a truly semi-infinite solid and hence real continuous spectra. In this way a detailed analysis of discrete and resonant states is provided. We mainly describe the embedding method and provide examples to compare the two approaches. We focus next on the structural and electronic properties of alkali adatoms. The adsorption structure of Na/Cu(001) at low coverages is calculated within the supercell geometry motivated by the results of the Cambridge group on surface diffusion by ^{3}He spin echo scattering. The dispersion, energy, effective mass, and width of surface (quantum well and image) states of alkali atoms on Cu(111) are worked out by the embedding approach and compared with experiments.

(Some figures in this article are in colour only in the electronic version)

Contents

1. Introduction

In the last decade the improvement of calculation facilities has stimulated the development of first-principles investigations, which have allowed the studying of a wide variety of complex systems in much detail. Such methods are advantageous because they do not explicitly depend on fitted parameters, and often disclose unexpected results of predictive nature. Much attention has been devoted to those systems which lack three-dimensional (3D) translational invariance, from biological molecules to clusters, from quantum dots, wires, and wells to nanotransport, from high Miller index surfaces to adsorbates.

In this paper we shall deal with theoretical treatments of adsorption within a first-principles framework. In such a case the system to be considered is semi-infinite in the direction orthogonal to the surface and one cannot take advantage of Fourier transforms as for periodic bulk materials. Most currently, one forces the problem to a finite size and 3D periodicity by making the calculation in the supercell framework. However, the repeated supercells, which describe an array of finite systems, may not be most appropriate to take into account some important features of surfaces: states in resonance with a continuum of substrates ones [1], phenomena such as adatom-induced resistivity, which requires the treatment of electron–hole pair excitations of arbitrarily small energy [2], and the effects of external fields and electron transport [3] are just a few examples. All of them require treating a really semi-infinite system. For this purpose Green function methods are most appropriate. In these approaches one solves the electronic problem, for example in the density functional theory (DFT) framework, only in a reduced volume, and matching with the solution in the extended substrate is suitably taken into account. Several approaches have been developed on the basis of the Dyson equation [4], such as the matrix method in [5] or the recursive Green function procedure recently applied to compute the width of adsorbate states [6]. A promising contribution has been just proposed [7] where the presence of the substrate is introduced as a boundary condition to the Kohn–Sham (KS) equations for the wavefunction, which must be solved in real space.

In this work we will concentrate on a different Green function method, the embedding one [35]. It accounts for the extended substrate by a non-local potential, called the embedding potential, defined at the boundary of a fairly limited region in which the DFT calculation is carried out. Such an 'embedded' region contains the perturbation due to a defect, e.g. the surface, or an adsorbate film. This approach is in principle exact: the approximations are only related to imperfect screening of the perturbation inside the embedded region and to the usually adopted exchange–correlation functionals of DFT.

Then we shall deal with alkali adatoms on metals, since they represent a benchmark system to study adsorption. Their investigations date back to studies of Cs on W by Taylor and Langmuir [8], who regarded such a system as an example of ionic adsorption causing a consistent reduction of the metal work function. Their findings were confirmed by the quantum mechanical model of Gurney, which casts the main features of alkali adsorption, later developed by other workers (for a review see [9]). At very low coverages, θ, the outer s level of the alkali adatom is broadened into a resonance, and charge is transferred from the adatom to the metal. This contributes to the formation of an induced dipole moment opposite to that of the surface and producing the decrease of the work function. Dipoles associated with adatoms interact in a repulsive way and arrange with possibly the largest interatomic distance. At increasing coverage, in order to lower the repulsive interaction, charge is transferred back to the adatom, producing a depolarization effect which diminishes the dipole moment: hence one observes saturation and eventually an increase of the work function.

In addition, experiments and first-principles calculations on a periodic solid have later provided a more complex picture. For example, a large change in the electronic configuration

at the surface does not result in a change of the bondlength; top site adsorption only occurs on close packed surfaces; rumpling may be necessary to increase the coordination of the adatom [9, 10]. A complete monolayer of alkali adatoms on metals has metallic character, and the metallization transition has been measured, as function of θ, by an increase of the deexcitation rate of metastable He and the subsequent filling of the alkali metal valence band [11]. Very recently a surprising band splitting induced by the adatom localized state has been reported [12].

It is also well known that, owing to the reduction of the work function of the system, alkali adatoms are good promoters of catalytic reactions. This phenomenon is observed for catalysts ranging from noble to transition metals for various molecules: examples are the dissociation of O_2, NO, and CH_4, oxidation of CO and methanol synthesis. Recent calculations show that Cs on Pt clusters dissociates H_2 with no surface barrier [13] and that a Cs overlayer on InPt(110) increases the oxidation rate by 13 orders of magnitude with the formation of phosphate $InPO_4$ [14], and that alkali adsorption may determine a softening of adsorbed molecule stretching mode [15].

Alkali atoms, at low coverages, are also good prototypes to study surface diffusion and adatom lateral interactions [16]. To this purpose an experimental tool is the quasi-elastic spectra of He scattering off the surface [17]. In this respect the ^{3}He spin echo technique, developed by the Cavendish Group at Cambridge [18, 19], working also in the time domain, is expected to supply a new deal of information on this topic.

Many investigations are also devoted to alkali atom surface states on noble metal surfaces which may display a gap in the projected band structure like copper (111). If so, quantum well states (QWSs) occur. Such states are usually probed by photoemission [20] and scanning tunnelling spectroscopy (STS) [21, 22] techniques. Since the QWS energies are tunable with the film thickness, alkali atom overlayers could also be relevant for perspective applications in electronics [23]. Excited states, measured by inverse (IPE) [24] and two-photon photoemission (2PPE) [25], are important too, being related to charge transfer and hence reactivity at surfaces [26]. Among them image states display interesting spectroscopic properties.

All these reasons have motivated several theoretical studies of alkali adatoms in the DFT framework [27–31]. Regarding image state calculations, many-body treatments beyond DFT have concentrated so far on lifetimes of electrons at free surfaces [32, 33].

It is therefore clear that alkali adatoms are an important subject of research. But their various properties cannot be computed most conveniently by using a single *ab initio* method. We shall present results of the structure and the energetics of Na/Cu(001) at very low coverages, worked out by a supercell calculation, and we will make use of the embedding approach for the investigation of the electronic surface state properties of Na and Cs on Cu(111).

In section 2, we shall describe the theoretical approaches. After a short presentation of the supercell method, we shall concentrate on the embedding one and shall illustrate their application by a few examples. The first part of section 3 will be devoted to the adiabatic properties of Na/Cu(001), and its second part to a detailed analysis of the quantum well and image states of alkali adatoms on Cu(111). Finally, the last section is intended for discussion and conclusions.

2. Theoretical approaches for adsorption

Currently the most used geometry for adsorption phenomena is the slab one. One recovers a fictitious periodic system by repeating slabs in the orthogonal direction, separated by a portion of vacuum, and can use standard methods for 3D periodic systems, i.e. the usual supercell geometry [34]. If the interaction of electrons with nuclei is described by pseudopotentials, it is

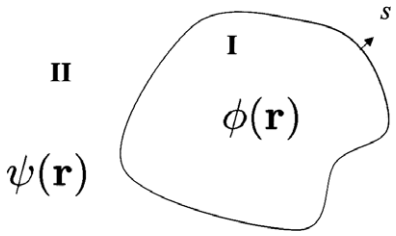

Figure 1. Embedding geometry. For details see the text.

convenient to expand the electronic wavefunctions via a plane wave basis set. The Hamiltonian matrix elements can be worked out in a straightforward way and one can obtain the ground-state properties of the system, i.e. its structure, energetics, and generally also the electronic states with very good accuracy within the DFT.

Slabs are finite systems in the direction normal to the surface, so their states are discrete ones at fixed parallel momentum. There are, however, surface properties in which the truly semi-infinite solid and hence the continuum of states should be included in the theory. In particular, to study the dispersion of the surface electronic states we wish to use a method capable of distinguishing between discrete or resonant structures. In this respect, as pointed out in the introduction, a most appropriate method is the embedding approach, which allows for the solution of the one-electron Schrödinger equation for a wide class of systems, in which a localized perturbation or defect is introduced in an extended substrate. By this method one can solve the Schrödinger equation in the defect region only, still accounting for the extended solid, and hence for a continuum of states. Following Inglesfield [35], this can be achieved by constructing an operator, the so-called embedding potential, which supplies the correct boundary conditions. In this way the solution within the embedded region I containing the perturbation will match properly the solution, assumed to be known, in the outer extended region II. A picture of the embedding geometry for an arbitrary system is displayed in figure 1.

To derive such an effective Schrödinger equation, we use the variational principle. First we construct a trial wavefunction Ψ built up of an arbitrary function ϕ in region I and of a solution ψ of the Schrödinger equation in region II at some trial energy ϵ. On the surface S, which divides regions I and II, the trial function is continuous, $\phi(\mathbf{r}_s) = \psi(\mathbf{r}_s)$, but a discontinuity in the derivative is permitted. Then, we look for a regular solution Ψ which minimizes the expectation value of the Hamiltonian H in the whole space. This expectation value is given by

$$E[\phi, \epsilon] = \frac{\int_{\mathrm{I}} \mathrm{d}\mathbf{r}\, \phi^* H \phi + \epsilon \int_{\mathrm{II}} \mathrm{d}\mathbf{r}\, \psi^* \psi + \frac{1}{2} \int_S \mathrm{d}\mathbf{r}_s\, (\phi^* \partial_{n_s} \phi - \psi^* \partial_{n_s} \psi)}{\int_{\mathrm{I}} \mathrm{d}\mathbf{r}\, \phi^* \phi + \int_{\mathrm{II}} \mathrm{d}\mathbf{r}\, \psi^* \psi}, \qquad (1)$$

where n_s is the unit vector normal to the infinitesimal surface element $\mathrm{d}\mathbf{r}_s$ pointing out of region I and ∂_{n_s} denotes $\frac{\partial}{\partial n_s}$. We make use of the Green function $G_0(\mathbf{r}, \mathbf{r}', \epsilon)$ for region II, which satisfies the following equation:

$$[H_0 - \epsilon] G_0(\mathbf{r}, \mathbf{r}', \epsilon) = \delta(\mathbf{r} - \mathbf{r}') \qquad \mathbf{r}, \mathbf{r}' \in \mathrm{II}, \qquad (2)$$

where $H_0 = -\frac{1}{2}\nabla^2 + V(\mathbf{r})$ is the Hamiltonian in region II. Unless stated otherwise, we use Hartree atomic units with $e = m_e = \hbar = c = 1$ throughout this paper.

The absence of the region I in (2) allows for free boundary conditions of the Green function on the surface S. By setting the normal derivative of $G_0(\mathbf{r}, \mathbf{r}', \epsilon)$ to zero on S (Neumann's boundary condition), we obtain the generalized logarithmic derivative condition

on the wavefunctions at the surface of the embedded region, and we can express $\partial_{n_s}\psi(\mathbf{r}_s)$ in terms of $\psi(\mathbf{r}_s)$ that we have assumed equal to $\phi(\mathbf{r}_s)$:

$$\frac{\partial\psi(\mathbf{r}_s)}{\partial n_s} = -2\int_S \mathrm{d}\mathbf{r}'_s\, G_0^{-1}(\mathbf{r}_s, \mathbf{r}'_s, \epsilon)\phi(\mathbf{r}'_s). \tag{3}$$

In equation (3), G_0^{-1} is the surface inverse of the substrate Green function satisfying Neumann's condition at the embedded surface. By inserting (3) into (1) and by minimizing $E[\phi, \epsilon]$ with respect to variations in ϕ, one obtains the required solutions of the problem in region I:

$$\begin{aligned}\left[-\frac{1}{2}\nabla^2 + \frac{1}{2}\delta(\mathbf{r}-\mathbf{r}_s)\frac{\partial}{\partial n_s} + V(\mathbf{r})\right]\phi(\mathbf{r}) \\ + \delta(\mathbf{r}-\mathbf{r}_s)\int_S \mathrm{d}\mathbf{r}'_s\left[G_0^{-1}(\mathbf{r}_s, \mathbf{r}'_s, \epsilon) + (E-\epsilon)\frac{\partial G_0^{-1}(\mathbf{r}_s, \mathbf{r}'_s, \epsilon)}{\partial\epsilon}\right]\phi(\mathbf{r}'_s) \\ = E\phi(\mathbf{r}) \qquad \mathbf{r}\in \mathrm{I}.\end{aligned} \tag{4}$$

We observe that $G_0^{-1}(\mathbf{r}_s, \mathbf{r}'_s, \epsilon)$ is an effective non-local, energy-dependent surface potential, the so-called embedding potential which guarantees the correct matching of the wavefunctions inside and outside S. The presence of the embedding potential in (4) confines the treatment of the infinite substrate within the embedded region. Such a potential is to be evaluated at an energy ϵ close to the eigenvalue E, since the integrand in (4) is the linear approximation to $G_0^{-1}(\mathbf{r}_s, \mathbf{r}'_s, E)$. The potential $V(\mathbf{r})$ can be taken as the one-electron effective potential of the KS scheme of DFT, in which the embedding method is numerically implemented. For the description of states at energy E belonging to the continuum part of the spectrum, we compute the embedding potential at energy $\epsilon = E$ so that the second term in the square brackets of (4) disappears. In this case we can verify that ϕ and ψ satisfy the Schrödinger equation at the same energy E in their region of definition and join together on S with continuous amplitude and derivative.

A convenient formalism in which discrete and continuum states can be treated on the same footing is the one based on Green functions. The one-particle Green function, in the embedding method, is the solution of

$$\begin{aligned}\left[-\frac{1}{2}\nabla^2 + v_{\mathrm{eff}}(\mathbf{r}) - E\right]G(\mathbf{r}, \mathbf{r}', E) \\ + \delta(\mathbf{r}-\mathbf{r}_s)\left[\frac{1}{2}\frac{\partial G(\mathbf{r}_s, \mathbf{r}', E)}{\partial n_s} + \int_S \mathrm{d}\mathbf{r}''_s\, G_0^{-1}(\mathbf{r}_s, \mathbf{r}''_s, E)G(\mathbf{r}''_s, \mathbf{r}', E)\right] \\ = \delta(\mathbf{r}-\mathbf{r}') \qquad \mathbf{r}, \mathbf{r}' \in \mathrm{I}.\end{aligned} \tag{5}$$

From the Green function, one can define the quantities of physical interest. First the local density of states (LDOS), $\sigma(\mathbf{r}, E)$ is defined by

$$\sigma(\mathbf{r}, E) = \frac{1}{\pi}\,\mathrm{Im}\, G(\mathbf{r}, \mathbf{r}, E + \mathrm{i}\delta), \tag{6}$$

where $\mathrm{i}\delta$ is a small imaginary energy. The charge density $\rho(\mathbf{r})$ is found by contour integration in the complex plane up to the Fermi energy E_{F}:

$$\rho(\mathbf{r}) = \frac{1}{\pi}\,\mathrm{Im}\int_c \mathrm{d}z\, G(\mathbf{r}, \mathbf{r}, z). \tag{7}$$

The density of states (DOS) is obtained from the spatial integration of the LDOS on the volume V of interest:

$$\sigma(E) = \int_V \mathrm{d}\mathbf{r}\,\sigma(\mathbf{r}, E). \tag{8}$$

In the calculations it is customary to expand G on a basis set $\{\chi_l(\mathbf{r})\}$:

$$G(\mathbf{r}, \mathbf{r}', E) = \sum_{lm} G_{lm}(E)\chi_l(\mathbf{r})\chi_m^*(\mathbf{r}'). \tag{9}$$

Inserting this expansion in (5) and integrating over the embedded region, we obtain the matrix equation

$$\sum_m \{H_{lm} + [G_0^{-1}(E)]_{lm} - ES_{lm}\}G_{mn}(E) = \delta_{ln}, \tag{10}$$

where

$$H_{lm} = \int_{\mathrm{I}} \mathrm{d}\mathbf{r}\, \chi_l^*(\mathbf{r}) H \chi_m(\mathbf{r}) + \frac{1}{2}\int_S \mathrm{d}\mathbf{r}_\mathrm{s}\, \chi_l^*(\mathbf{r}_\mathrm{s}) \frac{\partial \chi_m(\mathbf{r}_\mathrm{s})}{\partial n_\mathrm{s}}, \tag{11}$$

$$[G_0^{-1}(E)]_{lm} = \int_S \mathrm{d}\mathbf{r}_\mathrm{s} \int_S \mathrm{d}\mathbf{r}'_\mathrm{s}\, \chi_l^*(\mathbf{r}_\mathrm{s}) G_0^{-1}(\mathbf{r}_\mathrm{s}, \mathbf{r}'_\mathrm{s}, E)\chi_m(\mathbf{r}'_\mathrm{s}), \tag{12}$$

$$S_{lm} = \int_{\mathrm{I}} \mathrm{d}\mathbf{r}\, \chi_l^*(\mathbf{r})\chi_m(\mathbf{r}). \tag{13}$$

H_{lm} is the matrix element of the Hamiltonian in the embedded region plus the surface derivative term; $[G_0^{-1}(E)]_{lm}$ is that of the embedding potential; and S_{lm} is the overlap matrix element. We have the freedom to choose any convenient basis set whose elements represent a wide class of physically meaningful wavefunctions within the region of interest, and do not satisfy any particular boundary condition on S. In this way they have enough flexibility to span a wide range of values of $\phi(\mathbf{r}_\mathrm{s})$ and $\partial_{n_\mathrm{s}}\phi(\mathbf{r}_\mathrm{s})$.

It is interesting to make connection between the embedding approach and the Dyson equation one. Following the work by Baratoff and Schlüter [36], Ishida and Trioni [37] define an 'embedding' matrix operator by

$$\Sigma_{mn} = ES_{mn} - (H_0)_{mn} - (G_0)_{mn}^{-1}. \tag{14}$$

Note that the matrix element $(G_0)_{mn}^{-1}$ refers to the inverse of the unperturbed Green function G_0 defined in (2) not to the embedding potential. Using (14), the Dyson equation can be written as

$$\sum_m [H_{lm} + \Sigma_{lm} - ES_{lm}](G^\mathrm{D})_{mn} = \delta_{ln}, \tag{15}$$

where G^D labels the Dyson Green function solution. Equation (15) coincides with the embedding equation (10) if Σ is replaced by a term V^E defined as the sum of the embedding potential plus the normal derivative term. Σ and V^E are related by

$$(V^\mathrm{E})_{ln} = \Sigma_{ln} + \delta h_{ln}, \tag{16}$$

where δh arises because of the incompleteness of the basis set and vanishes for exact expansions. Such a result is expected, since both methods are a different way to write down the Schrödinger equation which can be derived by a variational approach. However, convergence to the right result may not be the same for each method. We observe that, in order to evaluate G correctly by the embedding method, it is sufficient to achieve a good accuracy in the expansion of G_0^{-1} on the embedding surface only (see (12)). On the contrary, in methods based on the Dyson equation, G_0^{-1} enters via an expansion on the full embedded volume. Therefore, the requirements on the basis set could be more stringent for the Dyson approach than for the embedding approach. Systematic investigations of convergence of both approaches do not exist. We only recall that for a simple model [37] it has been shown that the results of the two methods converge to each other rapidly inside the perturbed region by increasing the number of basis functions, while the Dyson equation method fails to incorporate the correct boundary

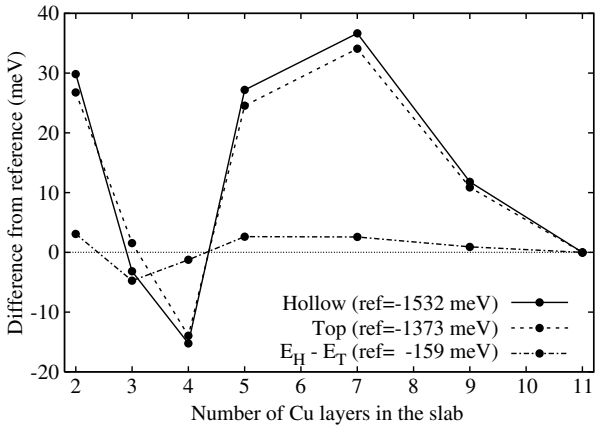

Figure 2. Adsorption energies for 0.5 ML of Na on Cu(001) in a supercell approach as a function of the slab thickness.

condition of the Green function at the surface S. In any case, the Dyson approach has been much more employed for computations at surfaces until a recent development of embedding by Ishida [38], which gives very accurate results for the energy-resolved properties at surfaces, and has been also extended to electron transport through an interface [39] and to tunnelling conductance [40]. In this method calculations of realistic surfaces and overlayers are performed within a full-potential linearized augmented plane wave (FLAPW) scheme, so the embedded region is partitioned into muffin tin (MT) spheres and an interstitial region. The embedding potential of a semi-infinite substrate is determined from the bulk crystalline potential by a self-consistent approach which avoids the prohibitive task of calculating it on complex curvy surfaces. For details see [38]. Calculations by embedding of a single isolated adatom are limited to the jellium substrate [41, 42].

We present now a few examples to critically examine how the supercell and the embedding approaches compare for different adsorbate properties. For computational details see the next section. First we discuss energetic properties. In this respect, we would like to remark that total energy calculations are more conveniently performed with the supercell geometry, since this fictitious system provides a framework in which the energy of the system and forces on the atoms can be computed in a straightforward way, and approximations introduced by the finite size in the orthogonal direction are usually under control. For example, figure 2 shows the relative adsorption energy of Na on Cu(001) at saturation coverage at the top adsorption site with respect to the most stable hollow one. This quantity quickly reaches an asymptotic value with a small number of layers in the slab. On the other hand, in embedding calculations of total energy, one has to take into account the interaction between the embedded region and the rest of the (infinite or semi-infinite) system, which implies difficult numerical integrations, because one has to include the effects of the perturbation induced by the defect in $\mathbb{R}^3$. In practice such calculations have only been accomplished for an atomic impurity in jellium [43]. In figure 3, we report the energy variation with respect to the asymptotic value E_0 of a substitutional Al defect in Mg jellium as a function of the radius of the embedded region, a sphere of radius R_{emb}. By confining the calculation of the total energy in the embedded region only (dotted line), one would miss the contributions from the long-range charge density oscillations induced in $\mathbb{R}^3$ by the atomic perturbation. The energy calculated in this way will converge to the correct value only slowly and in an oscillating manner, by increasing the size of the embedding region. On the other hand, by taking into account the long-range contributions, we obtain the solid line

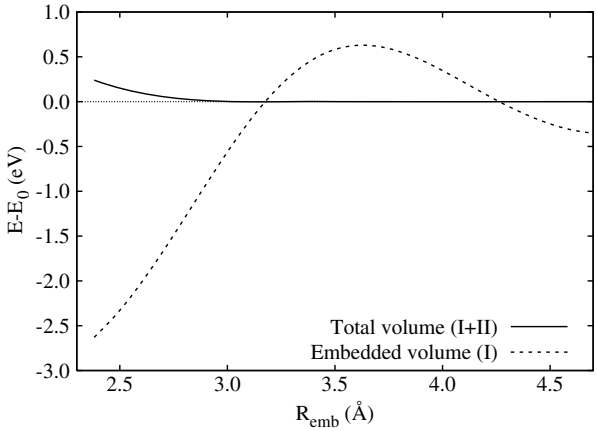

Figure 3. Energy variation with respect to $E_0 = -3.914$ eV of a substitutional Al defect in Mg jellium bulk as a function of the radius R_{emb} of the embedding sphere.

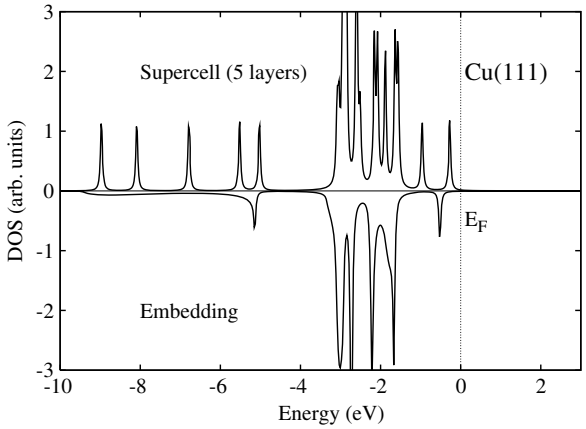

Figure 4. Comparison between the DOS at $\overline{\Gamma}$ calculated by the supercell and the embedding methods. Energies are measured from the Fermi level.

in figure 3, which converges rapidly and variationally with R_{emb}. However, implementing this procedure for more complex embedding geometries is a formidable task.

Second, we discuss electronic states. As an example we compare the DOSs calculated with the two approaches for a free Cu(111) surface. While the DOSs integrated in the surface Brillouin zone (SBZ) are fairly similar, the DOSs at $\overline{\Gamma}$ (or at any fixed $k_{\parallel}$) may display important differences. Figure 4 reports the DOSs obtained in the supercell and embedding approaches in the upper and lower panel, respectively (note that no dispersion in the direction normal to the surface is considered in the supercell geometry). In the DOS in the upper panel we observe a series of peaks; they represent discrete states and should be delta of Dirac, to which we have assigned a 0.025 eV width in order to be able to plot them. On the other hand, the DOS calculated by the embedding approach is a continuous function but an isolated peak appears at energies lower than E_{F}, i.e. at about -0.52 eV. Such a feature refers to a Shockley surface state within the surface-projected energy gap. This is indeed a surface discrete state which we have broadened as before in order to plot it. In the same energy range the supercell DOS displays

instead a double-peaked spurious structure which is due to the non-physical interaction between the two slab surfaces. Also the projected s band, in the energy range from −9 to −5 eV, is not well described in the supercell geometry.

In conclusion, while the shape of bulk-projected bands could be inferred also in the supercell approach from a careful convolution of the peaks, there is no simple way to distinguish between surface-projected and bulk-projected states within this geometry. One needs extra information, such as the analysis of the charge density, for distinguishing between continuous and discrete states. Though the supercell approach is much more popular due to its validity in obtaining adsorption structures and energetics and also to its simpler numerical implementation and use, a very careful determination and comparison of surface states with spectroscopic data may require the embedding method.

3. Alkali adatoms on copper

3.1. Adsorption energetics of Na on Cu(001)

Interpretation of adsorption experiments such as the ones presented by the Cambridge group and obtained by ^{3}He spin echo scattering measurements [19, 44] can be improved by coupling them to *ab initio* investigations. With this purpose, we have calculated the adsorption sites and the energetics of Na/Cu(001) at low coverages, in the framework of DFT. This is the first necessary step towards the description of complex inter-adatom interactions, and is included here because it nicely illustrates the application of the slab approach on a system for which no similar studies have been reported in the literature, to our knowledge.

The Cu surfaces have been modelled by a slab composed by five layers in periodically repeated supercells. Facing slabs are separated by a vacuum region of 11 Å (equivalent to six Cu(001) layers): such small values are already sufficient at low coverages, because the work function is still quite large and hence the charge density decays sufficiently rapidly in vacuum. Na atoms were adsorbed on only one side of the metal slab. Dipole field corrections were adopted to keep periodicity in the electrostatic potential without spurious electric fields inside the slab, as described by Bengtsson [45]. No significant change of structures and energetics were found without such correction, but its use is necessary in order to calculate changes in the work function upon Na adsorption. The two Cu layers farthest from the Na atoms were kept fixed at the bulk truncated positions, while the remaining atoms (including Na) were relaxed together with the underlying metal layer to minimize the Born–Oppenheimer potential energy. All the results presented in this work are obtained within a generalized gradient approximation for the exchange and correlation functional as proposed by Perdew, Burke, and Erznerhof (GGA-PBE) [46]. We used the plane-wave ultrasoft pseudopotential method [47], as implemented in the PWscf code of the Quantum-ESPRESSO distribution[4]. Pseudopotentials were derived from scalar-relativistic all-electron atomic calculations. Na and Cu pseudopotentials have 2s–2p–3s and 3d–4s valence electrons, respectively. Non-linear core corrections are used for Cu. Wavefunctions are expanded up to a kinetic energy cut-off of 27 Ryd; the effective potential and the charge density up to 216 Ryd. The SBZ zone integration has been performed with the Monkhorst–Pack [48] scheme, adopting $\mathbf{k}_\parallel$-point meshes equivalent to a 12×12 mesh in the irreducible surface unit cell of Cu(001).

The hollow site is the most stable adsorption site for Na adsorption on Cu(001). In a (4×4) unit cell, at nominal coverage $\theta = 1/16$ ML, the corresponding adsorption energy is

[4] Quantum-ESPRESSO (opEn-Source Package for Research in Electronic Structure, Simulation and Optimization, http://www.pwscf.org) is an initiative of DEMOCRITOS national simulation centre (http://www.democritos.it) for the development of open-source scientific software.

$E_{\rm ads}(1/16) = -1.67$ eV. The dependence of this adsorption energy on θ is mostly due, at low coverages, to the electrostatic dipole–dipole repulsion [49, 50]:

$$E_{\rm ads} = E_{\rm ads}^{(0)} + \frac{1}{N}\sum_{i<j}\frac{2\mu^2}{R_{ij}^3}, \tag{17}$$

where $E_{\rm ads}^{(0)}$ is the adsorption energy in the limit $\theta \to 0$, μ is the dipole moment of the Na atom which saturates at $\theta \to 0$, R_{ij} is the distance of two Na atoms, and the summation runs over all N adatoms in the system. Equation (17) can be easily specialized to the case where the atoms form a square lattice of side length $L = a/\sqrt{\theta}$ ($a = 2.57$ Å is the Cu–Cu distance), obtaining

$$\begin{aligned} E_{\rm ads}(\theta) - E_{\rm ads}^{(0)} &= \theta^{\frac{3}{2}}\frac{2\mu(\theta)^2}{a^3}\left[\frac{1}{2}\sum_{i\neq 0}\frac{1}{(R_{i0}/L)^3}\right] \\ &= \theta^{\frac{3}{2}}\mu_{[\rm D]}^2(\theta) \times 332 \text{ meV}, \end{aligned} \tag{18}$$

where $\mu_{[\rm D]}$ is the dipole expressed in Debye units. The quantity in square brackets, independent of coverage, amounts to 4.517. At 1/16 ML, our calculated work function of the Cu(001) surface is lowered by 1.12 eV, corresponding to a Na dipole of 3.14 D. By inserting these values into (18), we obtain an estimate of the adsorption energy for isolated adatoms: $E_{\rm ads}^{(0)} = E_{\rm ads}(1/16) - 51$ meV ≈ -1.72 eV.

Upon adsorption, the structure of the Cu surface is almost unaffected, as the atomic coordinates were found to change by at most 0.01 Å. The Na atom sits at 2.25 Å from the surface Cu layer. The potential energy of a single Na atom on Cu(001) was obtained by evaluating the adsorption energy $E_{\rm ads}$ in high-symmetry adsorption positions: hollow (H), bridge (B), and top (T), at coverage $\theta = 1/16$. Results are then extrapolated to zero coverage by using (18) to recover the isolated adatom limit. B and T positions are higher in energy than the H one, by 79 and 141 meV, respectively. Diffusion is thus easier along the [110] direction (H–B–H) than along [100] (H–T–H). This is consistent with the experimental findings by Graham *et al* [49]. By measuring the quasielastic peak width in He atom scattering and with the help of classical simulations based on the Langevin equation, they found that the best fit to the He data was given by 75 and 84 meV for the diffusion barriers through B and T sites. Such values are confirmed by simulations of the Cambridge group, parameterized in order to fit the ^{3}He spin echo data [44]. Note however, that while our value for adsorption in the B site is in good agreement with the experimental one for diffusion along [110], the result for the T site overestimates the corresponding Graham result for diffusion along [100].

As reported for the hollow site, the positions of the Cu atoms, upon adsorption in B and T sites, are very close to those of a clean surface, and thus not much perturbed by the presence of the Na adatom. There is still an appreciable effect on the surface Cu atoms right beyond Na. In the B case, they are pushed inwards by 0.04 Å, and the Na atom is 2.34 Å above the unperturbed surface Cu layer. For top site adsorption, the Cu atom under Na is pushed inwards by 0.12 Å, and the Na atom sits 2.39 Å from the Cu surface. Smaller relaxations are found in the second Cu layer, while coordinates of the third one (the last whose geometry was optimized) are not affected by Na adsorption at a level of 0.01 Å. Summarizing, the Cu surface looks rather flat for the large Na atom, the height corrugation being only 0.09 and 0.14 Å along [110] and [100], and almost rigid.

3.2. Spectroscopic properties on Cu(111)

In this second part of the section we mainly concentrate on the surface states of alkali adatoms on Cu(111), i.e. QWS and image states. The calculations are performed by the embedding

Table 1. Key features of the bound discrete states: the Shockley state (SS) of clean Cu(111) and the QWS of the $(3/2 \times 3/2)$ and (2×2) Na/Cu(111) systems, together with that for (2×2) Cs/Cu(111) one. Energies, measured with respect to the Fermi level, refer to $\overline{\Gamma}$.

	Calculated	Experimental
Clean Cu(111)—SS		[51]
Energy (eV)	−0.526	-0.434 ± 0.002
		-0.445 ± 0.05[a]
Effective mass (m_e)	0.445	0.43 ± 0.01
$(3/2 \times 3/2)$ Na/Cu(111)—QWS		[53]
Energy (eV)	−0.173	−0.127
Effective mass (m_e)	0.638	0.70 ± 0.04
(2×2) Na/Cu(111)—QWS		[24]
Energy (eV)	0.239	0.4
		0.410[b]
Effective mass (m_e)	0.809	0.64
(2×2) Cs/Cu(111)—QWS		[22]
Energy (eV)	0.027	0.040
Effective mass (m_e)	0.866	

[a] Reference [52].
[b] Reference [22].

method, while the structural parameters are extracted from the experimental data. We recall that the clean (111) surface of noble metals, such as Cu(111), is of particular interest because the projected band structure displays a wide energy gap at the $\overline{\Gamma}$ point of the SBZ where no bulk states are allowed but only the surface Shockley state which extends for most of the SBZ. Such a gap also prevents surface states from propagating into the bulk, while the electron system is a nearly 2D electron gas on the surface planes. These conditions generate a QWS on adsorption of alkali atoms whose properties have been widely studied experimentally and theoretically by DFT.

We start investigating Na adsorption by considering saturation coverage and a submonolayer one. At saturation (0.44 ML nominal coverage) a good consensus exists that the overlayer displays a $(3/2 \times 3/2)$ structure with the Na atoms occupying four nonequivalent hollow sites per $p(3 \times 3)$ unit cell. In the submonolayer regime the existence of an ordered phase is still debated [9, 10], but in the experiment by Dudde *et al* [24] a clear 2×2 pattern is reported, which should indicate the existence of a second phase corresponding to a nominal coverage of 0.25 ML. Subsequently, theoretical studies suggested the hollow site as the preferred adsorption one also for this $p(2 \times 2)$ structure [29]. Therefore we will discuss these two structures.

We now summarize the main parameters of the embedding calculation. The Green function was expanded using 10.24 Ryd as energy cut-off for the plane wave in the interstitial region. We set $l_{max} = 9$ for the spherical expansion inside the MTs, whose radii were chosen to be the same for the Cu and the alkali atoms, $r_{MT} = 1.27$ Å. The SBZ for the clean Cu(111) surface was sampled by a 16×16 regular mesh which was reduced to a set of 51 independent $\mathbf{k}_\parallel$ points; for adsorbed Na at saturation coverage the SBZ becomes nine times smaller and was sampled with a 6×6 mesh consisting of 10 independent $\mathbf{k}_\parallel$ points, while at smaller coverage ($\theta = 0.25$) it was sampled with a 10×10 mesh consisting of 22 independent $\mathbf{k}_\parallel$ points.

Figure 5 reports the adatom DOSs for the Na/Cu(111) $(3/2 \times 3/2)$ and (2×2) phases, by varying $\mathbf{k}_\parallel$ in the direction $\overline{\Gamma}$–$\overline{\mathrm{M}}$, in the upper and lower panel, respectively. At $\overline{\Gamma}$ the QWS appears as sharp peaks at −0.173 and 0.243 eV with respect to the Fermi level. Note that the QWS of Na at saturation is occupied while it is not in the other case, in agreement with

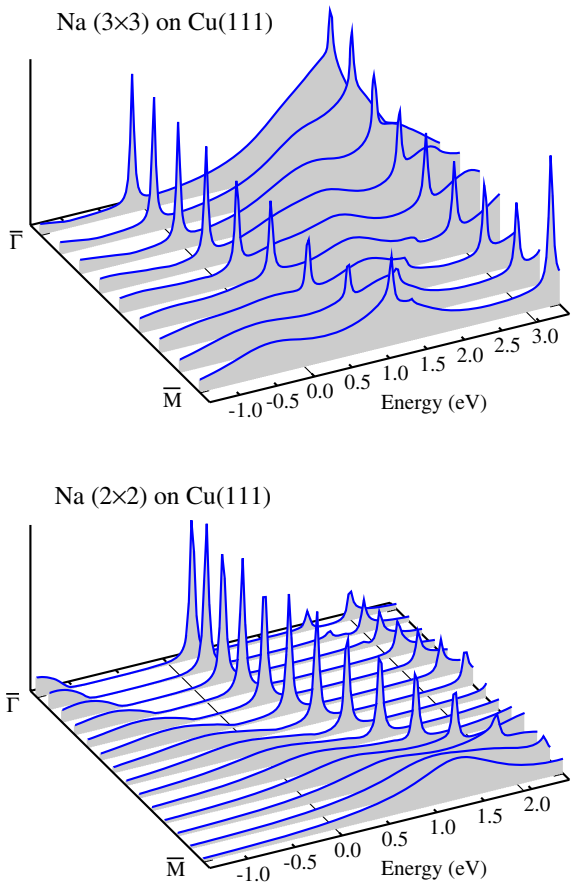

Figure 5. Dispersion of the QWS for two different Na coverages on Cu(111). Energies are measured from the Fermi level. In the calculation the peaks are broadened using $\delta = 0.025$ eV in (6).

the experiments [21, 24]. We point out that, differently from a supercell geometry, the use of the semi-infinite substrate allows for the presence of only one surface. So we do not observe any unphysical splitting of the overlayer states due to spurious interactions across the Cu slabs as already discussed for figure 4. The broad structure between 1 and 3 eV at the $\overline{\Gamma}$ point of Na/Cu(111) (3×3) is due to a 3s resonance of Na, nearly degenerate in energy with the 3p one. They are shifted above the Fermi level because of charge transfer to the substrate.

Table 1 contains the main features of these two adsorbate systems together with those for Cs adatom, and a comparison with experimental data. All the surface states are overbound, while there is a better agreement with experiments for the effective masses. In the upper panel of figure 5 a second surface band occurs at about 2.47 eV at $\overline{\Gamma}$, and disperses with an effective mass $m^* \approx m_e$. Such an energy is not in agreement with that of a second surface band, beyond the QWS, measured at 2.07 eV [24]. This structure, located outside the surface, is bound by the potential tail towards vacuum. Standard DFT is unable to properly reproduce the correct image form $v_{\rm eff}(z) = V_{\rm im}(z) \simeq -1/4z$ at large distance z, and such deficiency strongly affects this 'pseudo-image' state, as recently explained [31].

Within an *ab initio* framework one should resort to many-body techniques as done by Eguiluz [54] for the slab geometry and by Fratesi [55] for semi-infinite jellium in the embedding

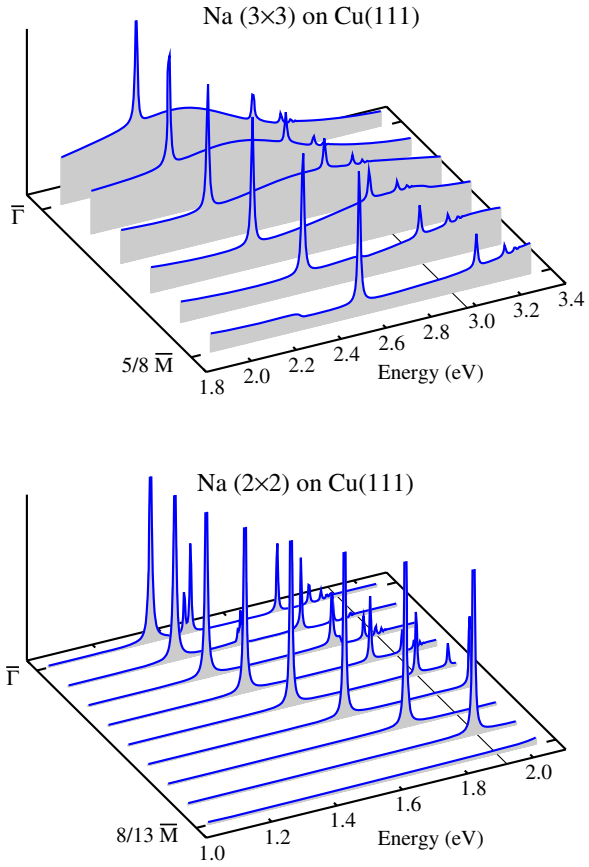

Figure 6. Dispersion of the image states for two different Na coverages on Cu(111). Energies are measured from the Fermi level. In the calculation the peaks are broadened using $\delta = 0.025$ eV in (6).

framework. However, in order to keep a lower computational cost, it is convenient to take advantage of the phenomenological approach introduced by Nekovee and Inglesfield [56, 57], which exploits the lack of periodicity of embedding in the z-direction. In practice, in the last step of the calculation, one takes into account the correct image potential behaviour in the construction of the embedding potential at the vacuum side, and lets the self-consistent potential v_{eff} merge smoothly into the image one in the outermost part of the embedded region [31]. We have performed the calculation of the image states in this framework. In the DOSs reported in figure 6, we can easily resolve the dispersion of the image states up to $n = 3$, differently from figure 5, in which the image tail was not considered. Note that the previously reported bound state at 2.47 eV is no longer present and that image states are correctly described. In particular the $n = 1$ state occurs at energy 2.21 eV and represents indeed the experimental one recorded at 2.07 eV. If such a state is measured with respect to the vacuum level, the agreement between theory and experiment is even better: -0.74 eV, to be compared with the experimental value of -0.72 eV. The apparent disagreement when energies are relative to the Fermi level can be ascribed to the difference between the measured and computed work functions (0.19 eV).

Table 2 summarizes the main findings for the first two image states of Na and Cs on Cu(111) at saturation coverage. The experimental data, obtained by two-photon photoemission,

Table 2. Key features of the first two image states of Cu(111) and Na/Cs on Cu(111) at saturation. Energies, measured with respect to the vacuum level, refer to $\overline{\Gamma}$.

		Calculated		Measured
System	State	Energy (eV)	Eff. mass (m_e)	Energy (eV)
Cu(111)	$n = 1$	−0.779	1.08	-0.82 ± 0.05[a]
	$n = 2$	−0.226	1.02	-0.25 ± 0.07[a]
Na/Cu(111)	$n = 1$	−0.742	1.02	-0.72 ± 0.03[b]
	$n = 2$	−0.223	1.01	-0.27 ± 0.03[b]
Cs/Cu(111)	$n = 1$	−0.665	0.90	
	$n = 2$	−0.246	0.98	

[a] Reference [58].
[b] Reference [59].

are in very good agreement with the theoretical ones. Note that the effective masses are close to one, since these states are farther away from the last Cu layer and their surface dispersion is nearly free-electron like.

The DOSs of the QWS (figure 5) and of the image states (figure 6) display a width, which is artificially magnified for plotting purposes. We observe that, because of the confinement of such states between two barriers, they lie within a gap of the projected bulk band of the clean Cu(111) surface. For this reason one should not expect any hybridization with the semi-infinite metal states. This would indeed be true for an unreconstructed (1×1) surface, but it is not valid any more when ordered overlayers change the periodicity of the surface. In reciprocal space, this corresponds to a mapping of the free SBZ onto that of the overlayer and results in backfolding of the electronic projected bands, since the periodicity is reduced. Consequently the QWS and the image ones of alkali adatoms on Cu(111) occur in energy regions of continuous bulk states, and should exhibit a finite linewidth differently from the Shockley state of Cu(111). Such a linewidth is usually called the elastic scattering contribution and is denoted by Γ_{elastic}. Of course other scattering processes could affect the linewidth of surface states of alkali adatoms. For this reason current investigations are also focused on the comparison of Γ_{elastic} with the electron–electron $\Gamma_{\text{e-e}}$ and electron–phonon $\Gamma_{\text{e-ph}}$ scattering processes. The various contributions, both measured and computed, to the width of the QWS of a p(2×2) overlayer of Na and Cs on Cu(111), have been reported in [22]. In particular, in that work Γ_{elastic} is computed by the recursive Green function procedure once the ground-state properties have been worked out by a standard supercell DFT approach.

For these systems the elastic linewidth is comparable to the other ones. As an example of a systematic study of Γ_{elastic} as a function of $k_{\parallel}$, in figure 7 we report the linewidth of Cs on Cu(111) calculated by the embedding method. We wish to stress that the computation has been performed with an imaginary part of energy equal to zero, so that no 'ad hoc' broadening is introduced. In the upper panel we show the dispersion of the QWS as a function of $k_{\parallel}$, while in the lower one Γ_{elastic} is depicted. At the $\overline{\Gamma}$ point the elastic width is about 2.5 meV, i.e. three times smaller than that calculated in [22]. Such a discrepancy is unexplained so far. In our opinion the estimate of the line width using two different computational steps as in [22] could generate some inaccuracy in projecting the wavefunctions, first expanded on a plane wave basis set, onto localized orbitals. In the lower panel of figure 7 observe that the full width at half maximum (FWHM) of the QWS rapidly increases on moving from the centre of SBZ. This effect is determined by the degree of hybridization between the surface state and the bulk ones. We also remark that the two different behaviours for $k_{\parallel}$ smaller or larger then 0.15 Å^{-1} are due to hybridization with one or with two projected bulk bands, respectively.

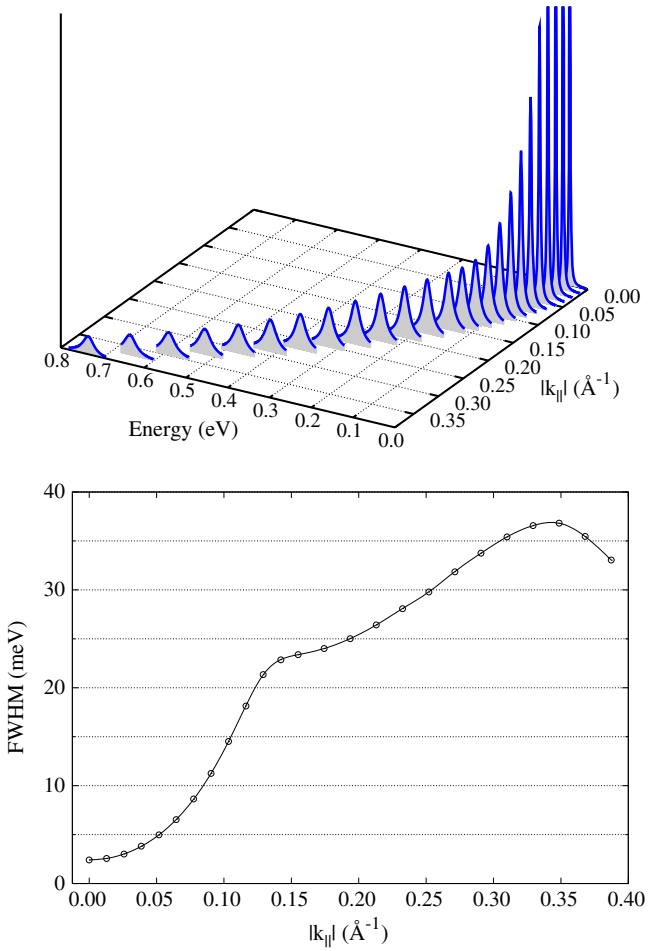

Figure 7. Dispersion of the QWS of (2 × 2) Cs/Cu(111). Energies are measured from the Fermi level. In the calculation $\delta = 0$ eV has been used in (6).

Also, the image states may display an elastic width. For example, for the $n = 1$ image state of K/Cu(111), our preliminary results indicate that Γ_{elastic} increases from 6 to 33 meV by varying $k_{\parallel}$ along the $\overline{\Gamma}$–$\overline{\text{M}}$ direction. For other systems such as the clean Cu(110) surface, the image states lie in the surface-projected bulk band. Consequently Γ_{elastic} for the resonance $n = 1$ is more than ten times larger and should dominate the linewidth [60].

4. Conclusions

In this paper we have presented an overview on how different *ab initio* methods, developed within the DFT framework, should be chosen in order to tackle the specific physical properties of adsorbates under investigation: the supercell approach supplies a 3D fictitious periodic system, in which calculations are generally simpler and the structure and the energetics are well converged with a very small number of atomic layers in the slab. Green function methods are needed to deal with a semi-infinite substrate and continuous states [4]. We focused on the embedding approach which allows for treating exactly the effects of an extended host by the

non-local, energy-dependent embedding potential, defined on the boundary of the localized region in which the DFT calculation is performed [35]. The construction of the embedding potential in the complex plane is usually a difficult task, and this explains the limited use of this approach. We deemed it important to provide an accurate description of embedding, also in view both of its recent numerical implementation to realistic systems [38], which provides an unprecedented clear description of surface states, and of its not yet exploited potentialities. Among them we recall the capability of treating isolated adsorbates and nanocontacts of molecular circuits without spurious periodicities.

The second focus of this work has been the calculation of the structure and electronic properties of alkali adatoms on copper. We reported theoretical results obtained with the supercell method for adsorption energies and structures of Na/Cu(001). These data are only a preliminary set up for further developments which will be dealing also with different adatom coverages. Though limited to an adiabatic picture, they should help in understanding the role of lateral interactions, and the possible presence of interesting new diffusion mechanisms. Here the new experimental method developed by the Cambridge group, i.e. the ^{3}He spin echo technique, looks very promising [18, 19], since the spectra obtained by ^{3}He atoms scattering off the surface should supply a much better resolution with respect to the ^{4}He ones.

As for electronic properties, we have demonstrated that several important measured quantities can be accessed with state-of-the-art methods based on the embedding procedure. In this way densities of states can be determined with no artificial broadening and accounting naturally for the substrate continuum spectrum. Surface states are then identified unambiguously, and their elastic broadening can be obtained with high accuracy. This enables us to distinguish between resonant and discrete states. In particular, a detailed analysis was reported here for the QWS on Cu(111), generated upon adsorption of alkali atoms. It is suggested that QWSs can be exploited for novel electronic devices [61]. In this respect, an accurate and predictive determination of their linewidth would be of crucial importance, and is beyond the realm of supercell calculations. The method applies with high precision to the determination of image states as well, provided the image tail at large distances is included phenomenologically in the *ab initio* effective potential.

It is important to remember that the comparison of numerical calculations, either based on the supercell or the embedding approach, with experiments where excited electronic states are probed, would in principle require a treatment beyond DFT, which is by definition a ground-state formalism. Excellent agreement with experiments can nevertheless be achieved in several cases, as shown here for example for the energy of image states. However, further investigations should also explicitly deal with excited surface states: to treat such a problem accurately, and from first principles, the embedding approach could be coupled to many-body methods.

Acknowledgments

This work was supported by the EU Network of Excellence NANOQUANTA (Grant No. NMP4-CT-2004-500198), and the MIUR of Italy (Grant No. 2005021433-003).

References

[1] Benesh G A and Inglesfield J E 1986 *J. Phys. C: Solid State Phys.* **19** L539
[2] Trioni M I, Ishida H and Brivio G P 2001 *Phys. Rev.* B **63** 075408
[3] Di Ventra M and Lang N D 2002 *Phys. Rev.* B **65** 045402
[4] Brivio G P and Trioni M I 1999 *Rev. Mod. Phys.* **71** 231
[5] Feibelman P J 1989 *Phys. Rev.* B **35** 2626

[6] Sànchez-Portal D, Ordejón P, Artacho E and Soler J M 1997 *Int. J. Quantum Chem.* **65** 453
[7] Abraham Y B and Holzwarth N A W 2006 *Phys. Rev.* B **73** 035412
[8] Taylor J B and Langmuir I 1933 *Phys. Rev.* **44** 423
[9] Diehl R D and McGrath R 1996 *Surf. Sci. Rep.* **23** 45
[10] Diehl R D and McGrath R 1997 *J. Phys.: Condens. Matter* **9** 951
[11] Fouquet P and Witte G 1999 *Phys. Rev. Lett.* **83** 360
[12] Liu C, Matsuda I, Hobara R and Hasegawa S 2006 *Phys. Rev. Lett.* **96** 036803
[13] Benitez J I, Castillo S, Poulain E and Bertin V 2006 *J. Chem. Phys.* **124** 024703
[14] Soukiassian P, Bakshi M H, Starnberg H I, Bommannavar A S and Hurych Z 1988 *Phys. Rev.* B **37** 6496
[15] Stolbov S and Rahman T S 2006 *Phys. Rev. Lett.* **96** 186801
[16] Ala-Nissila T, Ferrando R and Ying S C 2000 *Surf. Sci. Rep.* **40** 75
[17] Frenken J W, Hinch B J, Toennies J P and Wöll Ch 1990 *Phys. Rev.* B **41** 938
[18] Fouquet P, Jardine A P, Dworski S, Alexandrowicz G, Allison W and Ellis J 2005 *Rev. Sci. Instrum.* **76** 053109
[19] Alexandrowicz G and Jardine A P 2007 *J. Phys.: Condens. Matter* **19** 305001
[20] Fischer N, Schuppler S, Fischer R, Fauster Th and Steinmann W 1991 *Phys. Rev.* B **43** R14722
[21] Kliewer J and Berndt R 2001 *Surf. Sci.* **477** 250
[22] Corriol C, Silkin V M, Sànchez-Portal D, Arnau A, Chulkov E V, Echenique P M, van Hofe T, Kliewer J, Kröger J and Berndt R 2005 *Phys. Rev. Lett.* **95** 176802
[23] Milun M, Pervan P and Woodruff D P 2002 *Rep. Prog. Phys.* **65** 99
[24] Dudde R, Johansson L S O and Reihl B 1991 *Phys. Rev.* B **44** 1198
[25] Fischer N, Schuppler S, Fauster Th and Steinmann W 1994 *Surf. Sci.* **314** 89
[26] Kosloff R, Katz G and Zeiri Y 2000 *Faraday Discuss.* **117** 291
Kosloff R, Katz G and Zeiri Y 2000 *Faraday Discuss.* **117** 331
[27] Ishida H 1988 *Phys. Rev.* B **38** 8006
[28] Ishida H 2000 *Phys. Rev.* B **42** 10899
[29] Carlsson J M and Hellsing B 2000 *Phys. Rev.* B **61** 13973
[30] Torsti T, Lindberg V, Puska M J and Hellsing B 2003 *Phys. Rev.* B **66** 235420
[31] Butti G, Caravati S, Brivio G P, Trioni M I and Ishida H 2005 *Phys. Rev.* B **72** 125402
[32] Crampin S 2005 *Phys. Rev. Lett.* **95** 046801
[33] Borisov A G, Chulkov E V and Echenique P M 2006 *Phys. Rev.* B **73** 073402
[34] Payne M C, Teter M P, Allan D C, Arias T A and Joannopoulos J D 1992 *Rev. Mod. Phys.* **64** 1045
[35] Inglesfield J E 1981 *J. Phys. C: Solid State Phys.* **14** 3795
[36] Baratoff G A and Schlüter M 1986 *J. Phys. C: Solid State Phys.* **19** 4383
[37] Ishida H and Trioni M I 2001 *Phys. Rev.* B **63** 155108
[38] Ishida H 2001 *Phys. Rev.* B **63** 165409
[39] Wortmann D, Ishida H and Blügel S 2002 *Phys. Rev.* B **66** 075113
[40] Wortmann D, Ishida H and Blügel S 2005 *Phys. Rev.* B **72** 235113
[41] Trioni M I, Brivio G P, Crampin S and Inglesfield J E 1996 *Phys. Rev.* B **53** 8052
[42] Trioni M I, Marcotulio S, Santoro G, Bortolani V, Palumbo G and Brivio G P 1998 *Phys. Rev.* B **58** 11043
[43] Menchini C, Trioni M I and Brivio G P 2003 *Phys. Rev.* B **67** 035408
[44] Alexandrowicz G, Jardine A P, Hedgeland H, Allison W and Ellis J 2006 *Phys. Rev. Lett.* **97** 156103
[45] Bengtsson L 1998 *Phys. Rev.* B **59** 12301
[46] Perdew P, Burke K and Ernzerhof M 1996 *Phys. Rev. Lett.* **77** 3865
[47] Vanderbilt D 1990 *Phys. Rev.* B **41** 7892
[48] Monkhorst H J and Pack J D 1976 *Phys. Rev.* B **13** 5188
[49] Graham A P, Hofmann F, Toennies J P, Chen L Y and Ying S C 1997 *Phys. Rev. Lett.* **78** 3900
[50] Ellis J, Graham A P, Hofmann F and Toennies J P 2001 *Phys. Rev.* B **63** 195408
[51] Forster F, Nicolay G, Reinert F, Ehm D, Schmidt S and Häfner S 2003 *Surf. Sci.* **532–535** 160
[52] Kliewer J, Berndt R, Chulkov E V, Silkin V M, Echenique P M and Crampin S 2000 *Science* **288** 1399
[53] Kliewer J and Berndt R 2001 *Phys. Rev.* B **65** 035412
[54] Eguiluz A G, Heinrichsmeister M, Fleszar A and Hanke W 1992 *Phys. Rev. Lett.* **68** 1359
[55] Fratesi G, Brivio G P, Rinke P and Godby R W 2003 *Phys. Rev.* B **68** 195404
[56] Nekovee M and Inglesfield J E 1992 *Europhys. Lett.* **19** 535
[57] Nekovee M and Inglesfield J E 1992 *Prog. Surf. Sci.* **50** 149
[58] Wolf M, Knoesel E and Hertel T 1996 *Phys. Rev.* B **54** R5295
[59] Fischer N, Schuppler S, Fischer R, Fauster Th and Steinmann W 1993 *Phys. Rev.* B **47** 4705
[60] Quiniou B, Bulvović V and Osgood R M 1993 *Phys. Rev.* B **47** 15890
[61] Sentef M, Kampf A P, Hembacher S and Mannhart J 2006 *Phys. Rev.* B **74** 153407